

Chapter 12

Optimizing the Topology of Tendon-Driven Fingers: Rationale, Predictions and Implementation

Joshua M. Inouye, Jason J. Kutch and Francisco J. Valero-Cuevas

Abstract Tendon-driven mechanisms in general, and tendon-driven fingers in particular, are ubiquitous in nature, and are an important class of bio-inspired mechatronic systems. However, the mechanical complexity of tendon-driven systems has hindered our understanding of biological systems and the optimization of the design, performance, control, and construction of mechatronic systems. Here we apply our recently-developed analytical approach to tendon-driven systems [1] to describe a novel, systematic approach to analyze and optimize the routing of tendons for force-production capabilities of a reconfigurable 3D tendon-driven finger. Our results show that these capabilities could be increased by up to 277 % by rerouting tendons and up to 82 % by changing specific pulley sizes for specific routings. In addition, we validate these large gains in performance experimentally. The experimental results for 6 implemented tendon routings correlated very highly with theoretical predictions with an R^2 value of 0.987, and the average effect of unmodeled friction decreased performance an average of 12 %. We not only show that, as expected, functional performance can be highly sensitive to tendon routing and pulley size, but also that informed design of fingers with fewer tendons can exceed the performance of some fingers with more tendons. This now enables the systematic simplification and/or optimization of the design and construction of novel robotic/prosthetic fingers. Lastly, this design and

J. M. Inouye
Department of Biomedical Engineering, University of Southern California,
CA 90089, USA
e-mail: jinouye@usc.edu

J. J. Kutch
Division of Biokinesiology and Physical Therapy, University of Southern California,
CA 90089, USA
e-mail: kutch@usc.edu

F. J. Valero-Cuevas (✉)
Department of Biomedical Engineering and the Division of Biokinesiology
and Physical Therapy, University of Southern California, CA 90089, USA
e-mail: valero@usc.edu

analysis approach can now be used to model complex biological systems such as the human hand to understand the synergistic nature of anatomical structure and neural control.

Keywords Biologically-inspired robots • Mechanism design

1 Introduction

Bio-inspired robotic hands employ multiple robotic fingers for dexterous grasping and manipulation tasks [2–13]. Bio-inspiration can refer to their tendon-driven nature, but also the asymmetry of the routings, the variation in moment arm sizes, and the non-uniform distribution of maximal tendon tensions. Robotic finger kinematics may be anthropomorphic or they may be less complex to simplify the construction and control of the fingers. Moreover, two fundamental classes of actuation are typically used: (i) those that use remote actuation (e.g., motors outside the fingers which actuate tendons, cables, or gears) and (ii) those that use internal actuation (e.g., motors inside the fingers). Tendon-driven limbs and fingers are ubiquitous in vertebrates, and such bio-inspired tendon-driven actuation has proven engineering design advantages such as light weight, low inertia, small size, backdrivability, and design flexibility [14]. However, the mechanical complexity of tendon-driven systems (e.g., the large number of design parameters) has precluded the development of modeling, design, and analysis tools to optimize their performance, control, and construction. In this paper, we analyze, optimize, and test alternative implementations of a 3D tendon-driven robotic finger. We validate this approach with physical hardware implementations from the functional perspective of maximizing the set of feasible endpoint static forces.

Many considerations go into the design of robotic fingers and hands, such as force and velocity production, control, ease of construction, design simplicity, and cost. Adequate force-production capabilities are a necessary element of the multidimensional design puzzle: according to Firmani, “The knowledge of maximum twist and wrench capabilities is an important tool for achieving the optimum design of manipulators” [15]. In fact, if a finger cannot produce sufficient endpoint force while meeting other critical design requirements such as size and number of motors (for example in space, hazardous or surgical applications), then the mechatronic system is useless regardless of the attributes of the controller or ease of manufacturing. Therefore, as a demonstration of our novel modeling, analysis and optimization approach, we concentrate on the kinetostatic (endpoint force-production) capabilities for robotic fingers.

Several studies have analyzed the kinetostatic performance of tendon-driven and torque-driven manipulators [15–23] (determining the kinetostatic capabilities given design parameters), and several others have addressed their optimization or synthesis (specifying the design parameters given desired capabilities) [24–32].

These studies are based on mathematical theory. The fabrication of robotic fingers has been widely accomplished for robotic hands [2–13]. Experimental testing of kinetostatic performance can be found in the biomechanics literature [33, 34], but these do not implement a system whose parameters can be altered. We combine these three areas of *theory, fabrication, and testing* to optimize and validate hardware implementations of alternative robotic finger designs.

2 Nuances of Biological and Engineering Systems that are Tendon-Driven

Understanding the mechanical properties of tendon-driven plants is critical to understanding the actual problem confronting both brain-body dynamics and the plant-controller engineering design problem. Elsewhere we have shown the importance of understanding the nuances of tendon-driven systems that cannot be understood when applying the common torque-driven mathematical approach to the actuation of serial kinematic chains (i.e., limbs [35]). However, a brief summary is warranted because the present work is motivated by the need to understand well (i) the consequences of alternative tendon routings (i.e., system topologies) and their optimization; and (ii) the need to validate the analytical and computational approaches we have developed and promoted in prior work.

The nuances of tendon-driven systems include:

- *Topology matters*: When thinking of the structure and function of anatomical and engineering systems, it is important to distinguish between the topology of the system and its specific parameter values [36]. The topology consists of the type and connectivity of elements of any particular systems, which in this case include the number and type of kinematics degrees of freedom, and the way in which tendons cross and actuate joints. The specific parameters then include the actual number of limb segments, degrees of freedom, the kinematic connectivity across limb segments and the specifics of how many tendons there are, which kinematic degrees of freedom they cross and actuate, and the moment arm at each degree of freedom (assuming only rotational degrees of freedom). We have shown, for example, that apparently similar topologies can have very different mechanical capabilities [36], and that some topologies can be used to satisfy various functional goals [37]. Therefore the topology and parameters values of a tendon-driven system must be considered carefully.
- *Agonists, antagonists and co-contraction*: The perspective and language that emerges from analyzing single joint systems such as the elbow or knee are very often not valid in the case of multi-articular, multi-tendon systems [35]. More specifically, the idea that there is an agonist tendon that produces torque in the desired sense, which is opposed by an antagonist tendon on the “other side” of the joint does not extrapolate well. In the case of two or more kinematics degrees of freedom, each tendon produces a specific combination of joint

torques; and all constitute a basis for mechanical actions. The positive addition of their actions (muscles can only pull, not push) creates the set of feasible outputs; be they in the joint torque space (feasible torque set) or the end-point space (feasible wrench set). Thus the routing of each tendon and the strength of each muscle can dramatically affect the size and shape of the feasible actions of the system. In the multi-joint case, therefore, mechanical actions are a vector addition of these basis vectors, and it is no longer possible to label some muscles as agonists or antagonists. This is because all active basis vectors contribute to the task equally. That is, the loss of any one muscle will affect the ability to implement that solution. Similarly, the vector addition of all contributing vectors at times requires the simultaneous cancellation of mechanical actions at a joint [34]. This can lead to activity in muscles on opposite sides of a joint, which has often been called co-contraction by extrapolation from the single joint case. However, such simultaneous activity is not an optional strategy in the sense that co-contraction is usually thought of. Rather, such vector addition that engages muscles on either side of a joint is at times simply what is required to accomplish the task [38] and is not always a decision the nervous system makes to, for example, increase joint impedance, etc.

- *Muscle Redundancy and Synergies*: More recently we have called attention to the fact that muscle redundancy, while mathematically undeniable, does not necessarily imply robustness to muscle dysfunction [39]. That is, the solution space for a given task has a specific structure given by the constraints of the task [34]. This structure then defines which muscles must be active at a level higher than zero (and are therefore necessary); and which muscles are needed at moderate or high levels of activation (and therefore the task is sensitive to weakness or dysfunction of those muscles) [39]. Lastly, because the structure of the solution space is given by the interaction among the topology of the plant and the constraints of the task, it is not surprising (in fact, it is expected) that EMG and other recordings often exhibit a lower dimensional structure [40]. This structure depends directly on how many tendons there are, how they are routed, how they can be used to fulfill the constraints of the task and is not necessarily the consequence of a specific choice of neural control strategy. Disambiguating mechanically necessary versus neurally optional features of muscle coordination required using the techniques presented here to identify the solution space for a task given a specific tendon topology.

Therefore, our work here is motivated by the need to be able to test the functional and control consequences of any topology for a tendon-driven systems, be it biological or mechatronic. Moreover, the predictions and interpretations mentioned above depend to a certain extent on the validity of such linear methods to find and describe the structure of the solution space for static force production. Therefore, it is of critical interest to be able to validate these methodology predictions experimentally.

3 Finger Construction

We had several design requirements when designing a reconfigurable robotic finger as a test bed for analysis, optimization, and testing. They were

- (1) Ability to arbitrarily change tendon routing (i.e., the joints each tendon crosses, and whether they produce positive or negative torque at each joint).
- (2) Ability to vary pulley sizes (i.e., moment arms of the tendons).
- (3) Low friction.
- (4) Sufficient and well arranged degrees-of-freedom (DOFs) to allow three-dimensional endpoint motion and force production.
- (5) Robust, durable, rigid.

We designed the finger in SolidWorks 2010 (Dassault Systèmes), as shown in Fig. 1. The actual reconfigurable finger is also shown. It was constructed with one ad-abduction DOF and two flexion–extension DOFs. The primary materials were aluminum (for the links and terminating pulleys), turcite (for the spacers and rotating pulleys), and ball bearings with extended inner rings (mounted on all pulleys and link axes). All of the pulleys were custom-machined and two sizes were constructed for reconfigurability: a radius of 8.0 mm for the large pulleys and 4.4 mm for the small pulley, as shown in Fig. 2. There were multiple pulleys that had to be added between the axes to ensure reconfigurability of the tendon routing (i.e., that each tendon could rout on either side of every joint and no bowstringing of the tendons would occur).

The selection of link lengths and pulley sizes was otherwise fairly arbitrary, and since our study did not involve optimization of incremental changes in these parameters (except the 2 pulley sizes), we simply constructed it to have reasonable size that could be fabricated and tested.

4 Methods

After construction of the finger with the desired capabilities, we were then able to analyze and optimize tendon routing and pulley sizes based on the actual kinematics and reconfiguration options of the finger.

4.1 Force Polytope Analysis

Quantification of the force-production capabilities of a robotic finger (or manipulator) can be accomplished by determination of the feasible force set (or force polytope) of the finger. This convex set encloses all feasible forces that the fingertip can exert given kinematic parameters, tendon routing and pulley sizes, and

Fig. 1 2-D and 3-D views of finger model in solidworks, and the actual finger

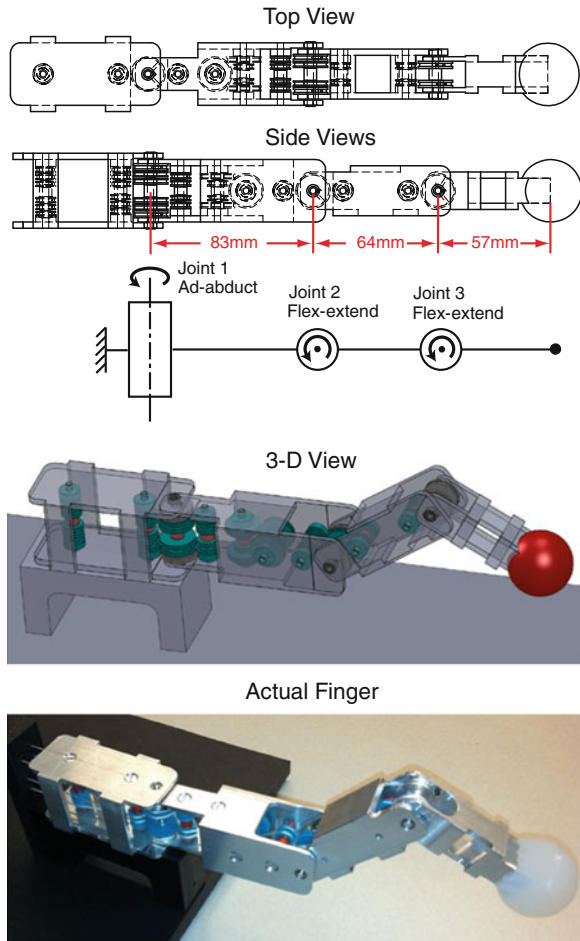


Fig. 2 Pulleys used in finger design. **a** Turcite rotating small pulley. **b** Aluminum terminating small pulley. **c** Turcite rotating large pulley. **d** Aluminum terminating large pulley

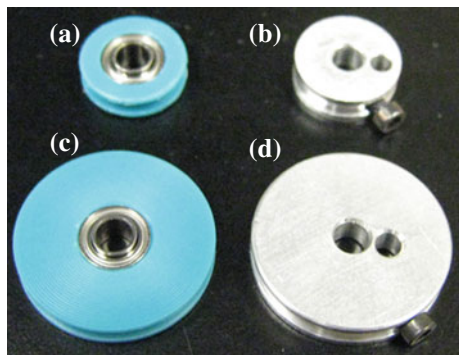
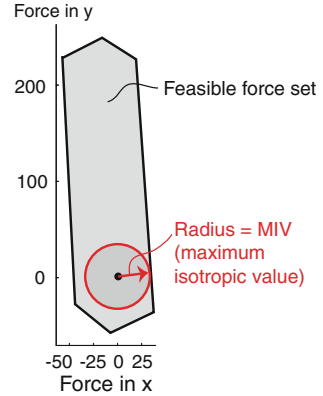


Fig. 3 Illustration of calculation of MIV (maximum isotropic value) from feasible force set



maximal tendon tensions. A quality metric that can be assigned to this set is known as the maximal isotropic value (MIV) [18]. Since we are not assuming any specific task that this finger must perform, then we chose to use this metric. We could have used any other metric instead of the MIV. Further comments can be found in the discussion section. The MIV is the radius of the largest ball, centered at the origin, that the feasible force set can contain, as illustrated in Fig. 3 for a 2-D feasible force set. A finger can exert at least that many units of force in any direction.

We can use an activation vector, \vec{a} , to represent the degree to which a tendon is activated. Each element of \vec{a} ranges between 0 (no activation, zero force) and 1 (full activation, maximal force). Further discussion may be found in [35]. If we define F_0 as a diagonal matrix of maximal tendon tensions, R as the moment arm matrix (or structure matrix) relating tendon tensions to joint torques, and J as the posture-dependent Jacobian relating joint velocities to fingertip velocities, then we can get the fingertip force vector \vec{f} from tendon activations [34] if the Jacobian is square and invertible:

$$\vec{f} = J^{-T} R F_0 \vec{a} = A \vec{a} \quad (1)$$

For a given fixed finger posture, the J^{-T} , R , and F_0 matrices can be grouped into a linear mapping from activations into fingertip force, which we call an action matrix A [34, 35]. Each column of A represents the force vector each tendon produces at the fingertip in that posture if fully activated. The collection of all such forces (i.e., all columns of matrix A) forms a set of output force basis vectors. Linearity of this mapping holds true for static forces because the Jacobian and moment arms remain constant. The Minkowski sum of these basis vectors forms the feasible force set of the fingertip, and can be computed by taking the convex hull of the points generated by mapping each vertex of the activation hypercube (i.e., each vertex of the unit hypercube in the positive orthant) to fingertip wrench space via the action matrix A [34].

There are two ways to describe a convex hull: (i) a set of vertices and (ii) a set of linear inequalities. Vertex enumeration methodologies can calculate one

description given the other. The Qhull software package uses the Quickhull algorithm [41] and is used to perform the MIV calculations in this study. Other vertex enumeration algorithms that can perform these calculations easily include CDD [42] and LRS [43].

The description involving a set of linear inequalities (similar to a linear programming inequality constraint formulation) takes the form

$$Ax \leq b \quad (2)$$

where A is a matrix of constants defining the inequalities, x is a vector of variables of length d , where d is the dimensionality of the convex hull, and b is a vector of constants. If we denote A_i as the i th row of A , then the linear inequality $A_i x \leq b_i$ defines a halfspace, which also defines a facet of the convex hull. The perpendicular (i.e., shortest) Euclidean distance (or offset) of this facet from the origin, in general, will be given by

$$\frac{b_i}{\|A_i\|_2} \quad (3)$$

The Qhull output, however, automatically sets each $\|A_i\|_2$ equal to 1, so the i th offset from the origin is simply the signed constant b_i . Calculation of the MIV in this study involves simply finding the minimum of b corresponding to the feasible force set.

For our finger, the Jacobian is a 3×3 matrix which is square and invertible in our experimental postures, R is a $3 \times \ell$ matrix (ℓ is the number of tendons, which is 4, 5, or 6), and F_0 is an $\ell \times \ell$ diagonal matrix of maximal tendon tensions.

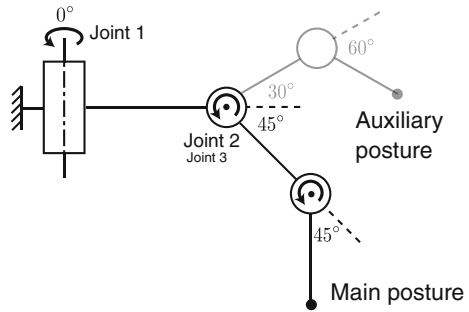
4.2 Evaluating Tendon Routings

The construction of the finger allowed for various moment arm matrices to be implemented which had 4, 5, or 6 tendons. These designs are known as $N + 1$, $N + 2$, and $2N$ designs, where N is the degrees of freedom of the finger. We enumerated all possible moment arm matrices beginning with the “base” matrices shown in Fig. 4. The $N + 2a$ and $N + 2b$ designs differ only in that the second tendon terminates at the first joint in the $N + 2a$ designs and at the second joint in the $N + 2b$ designs. We replaced each ‘#’ with either a 1 or -1 (in accordance with the sign of the moment exerted on a joint when the corresponding tendon is under tension; see Fig. 1 for definition of joint axes) in a full combinatoric search and then checked the controllability (i.e., that all of the joints could be actuated independently in torque and motion) conditions as described in [22]. We then calculated the MIV for these routings using the large pulleys in the main posture: 0° at joint 1, -45° at joint 2, and -45° at joint 3, as shown in Fig. 5. To make comparisons feasible across finger designs with different number of tendons, we used a uniform

Fig. 4 Base moment arm matrices used when finding admissible and unique tendon routings

<p style="text-align: center;">N+1 design: 24 admissible, 3 unique</p> $R = \begin{bmatrix} \# & \# & \# & \# \\ 0 & \# & \# & \# \\ 0 & 0 & \# & \# \end{bmatrix}$	<p style="text-align: center;">N+2a design: 88 admissible, 6 unique</p> $R = \begin{bmatrix} \# & \# & \# & \# & \# \\ 0 & 0 & \# & \# & \# \\ 0 & 0 & 0 & \# & \# \end{bmatrix}$
<p style="text-align: center;">N+2b design: 296 admissible, 11 unique</p> $R = \begin{bmatrix} \# & \# & \# & \# & \# \\ 0 & \# & \# & \# & \# \\ 0 & 0 & 0 & \# & \# \end{bmatrix}$	<p style="text-align: center;">2N design: 872 admissible, 20 unique</p> $R = \begin{bmatrix} \# & \# & \# & \# & \# & \# \\ 0 & 0 & \# & \# & \# & \# \\ 0 & 0 & 0 & 0 & \# & \# \end{bmatrix}$

Fig. 5 Finger posture used in computations and experimental testing



maximal tendon tension distribution, with the sum being constrained¹ to 60N (i.e., for designs with 4, 5, and 6 tendons, the maximal tensions were 15, 12, and 10N, respectively). We found that many of the admissible routings produced the exact same MIVs and feasible force set volumes, likely corresponding with structurally isomorphic routings [22]. The number of routings that produced unique MIVs was a very small subset of the admissible routings, as can be seen from the numbers in Fig. 4. In cases of optimization of a more complex finger or manipulator where the number of unique MIVs may be orders of magnitude higher, methods for selection of a subset for further optimization such as in [46] may be used.

¹ The sum of maximal tendon tensions being equal is an important constraint due to the size, weight, and motor torque (and therefore tendon tension) limitations inherent in dexterous hands. For example, the torque capacity of motors is roughly proportional to motor weight, and minimization of weight was an important consideration in the design of the DLR Hand II [44]. In addition, the maximal force production capabilities of McKibben-style muscles are roughly proportional to cross-sectional area [45]. Since the actuators typically will be located in the forearm, then the total cross-sectional area will be limited to the forearm cross-sectional area. In this study, for simplicity and without affecting the generalizability of our approach or results, we do not consider alternative constraints on the actuation system (e.g., electrical current capacity, tendon velocities, etc).

The total number of routings producing distinct feasible force sets² was 40. For each of those routings, we calculated the MIV for all combinations of large and small pulleys. For example, the $N + 1$ design has 9 moment arm values. Therefore, there are 2^9 combinations of large and small pulleys for that case. Taking the combination with the highest MIV for each routing gave 40 moment-arm-optimized routings. Therefore, we had 40 unoptimized routings and 40 optimized routings. Out of these 80, we chose 6 different routings to test experimentally in a fashion that permitted testing of a large range of MIVs, and included the design with the highest predicted MIV. Otherwise the selection was arbitrary.

4.3 Experimental Testing of Tendon Routings

For each of the tendon routings tested, we first arranged the pulleys and strings (0.4 mm braided polyester twine) to match the desired configuration. We then mounted the finger onto a base that was part of a motor array system as shown in Fig. 6. The DC motors were coupled to capstans on which the string wound. Each string was then routed around pulleys that were attached to load cells (Interface SML 25, Scottsdale, AZ) which provided force measurements for the closed-loop controller implemented in Realtime LabView. The endpoint of the finger was fixed to a custom made gimbal which constrained translational motion but not rotational motion (we did not want the fingertip to be over-constrained). The gimbal was attached to a 6-axis load cell (JR3, Woodland, CA). The sampling rate and control loop frequency were both 100 Hz.

A small pretension of 1N was applied to each string to remove slack and prevent it from falling off of the pulleys. Then each vertex of the activation hypercube (as described in the previous section) was applied to the strings (in addition to the pretension) in ramp-up, hold, and ramp-down phases to find the feasible force set [39]. As in prior work, [39], vertices of this experimental feasible force set were determined from the hold phases and then used to find the MIV using Qhull as described earlier. The experimental MIV could then be compared with the theoretical MIV (from computational results).

To compare the shapes of the experimental and theoretical feasible force sets, we first normalized the volume of the experimental feasible force set to make it equal to the volume of the theoretical feasible force set. We then calculated the mean Euclidean distance of each vertex from the theoretical feasible force set from

² Due to the nature of our full combinatoric search, moment arm matrices that produced mirrored feasible force sets about a plane passing through the origin (which would have the same MIV) were discarded and also those moment arm matrices that were produced by a rearrangement of the columns. For example, in Fig. 4, interchanging columns 5 and 6 does not change the feasible force set, it only reverses the “numbering” of the tendons. But in the full combinatoric search, both of these numberings would be different matrices producing identical feasible force sets.

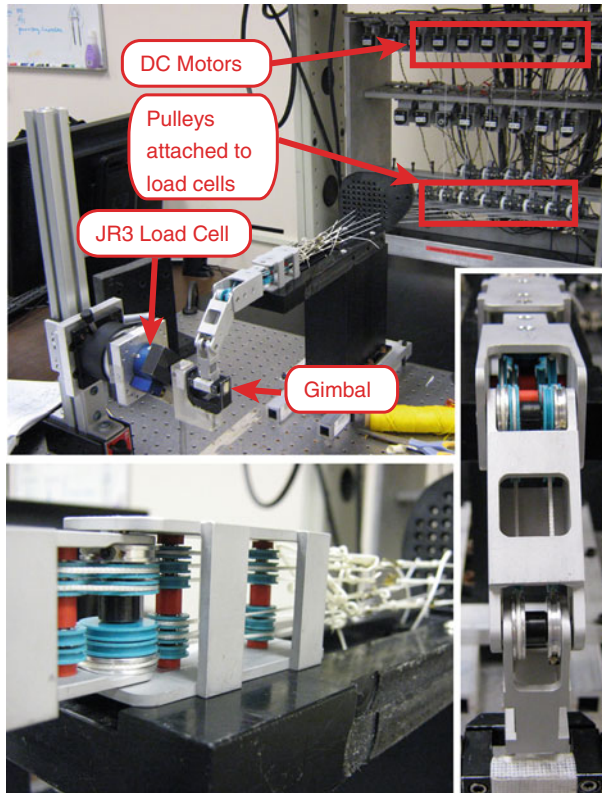


Fig. 6 Experimental system for feasible force set testing

the corresponding vertex in the experimental feasible force set. We did this because there was always friction loss in the experiment.³ In addition, we calculated the average angle between the two vectors (starting and the origin and ending at the corresponding vertex) formed from corresponding vertices.

We tested the finger in the main posture (for which we optimized MIV) and an auxiliary posture (to validate the predictions more fully). These postures are shown in Fig. 5. For each design and posture, we did three repetitions of tests. Since there were 6 designs, 2 postures, and 3 repetitions, we conducted a total of 36 tests.

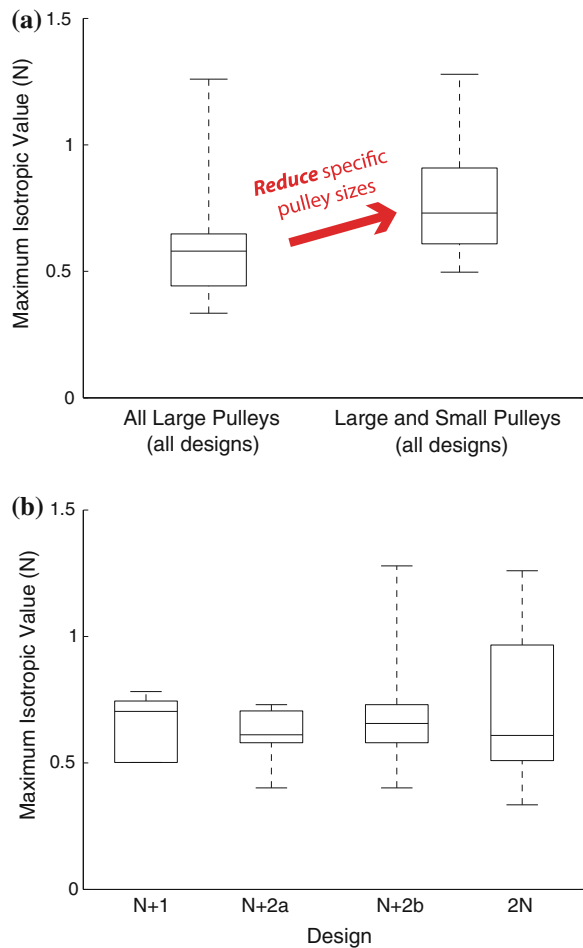
³ Take an extreme case in which friction loss was 50 % exactly for every tendon. The theoretical feasible force set is a unit cube. While the shape of the experimental feasible force set would be also an exact cube, it would be 50 % contracted in every direction and therefore the corresponding vertices would be far from each other. If we normalized the volume, the corresponding vertices would be in the same location, and the mean distance (in shape similarity) would be zero.

5 Results

5.1 Calculating Maximum Isotropic Values

The 40 unique unoptimized and 40 unique optimized routings produced the MIVs shown in Fig. 7a, b. Optimization of the pulley sizes increased the average MIV from 0.60 to 0.78N, a 30 % increase as shown in Fig. 7a, and the maximum increase for a routing by this optimization was 82 %. It is interesting to note that this force-production capability increase is achieved by simply decreasing specific pulley sizes in an informed manner. We can see from Fig. 7b that designs with 4 tendons could not produce MIVs higher than the best designs with 5 or 6 tendons. However, the best design with 4 tendons did have a higher MIV than many

Fig. 7 Maximum isotropic values for various routings. **a** Boxplot of MIV for all designs before and after pulley-size optimization. **b** Boxplot of MIV versus design (includes optimized and unoptimized pulley sizes)



alternative routings that had more tendons. In addition, the maximal increase from only rerouting tendons (no pulley size optimization) was 277 % (i.e., the increase from the worst admissible routing to the best admissible routing for a given number of tendons).

5.2 Theoretical Predictions Versus Experimental Results

The experimental results and the routings tested are shown in Fig. 8. The data points shown in Fig. 8b are averages of the three test repetitions in both the main posture and the auxiliary posture for each of the designs. The average standard deviation from the three test repetitions was very low at 0.0090N, showing that the

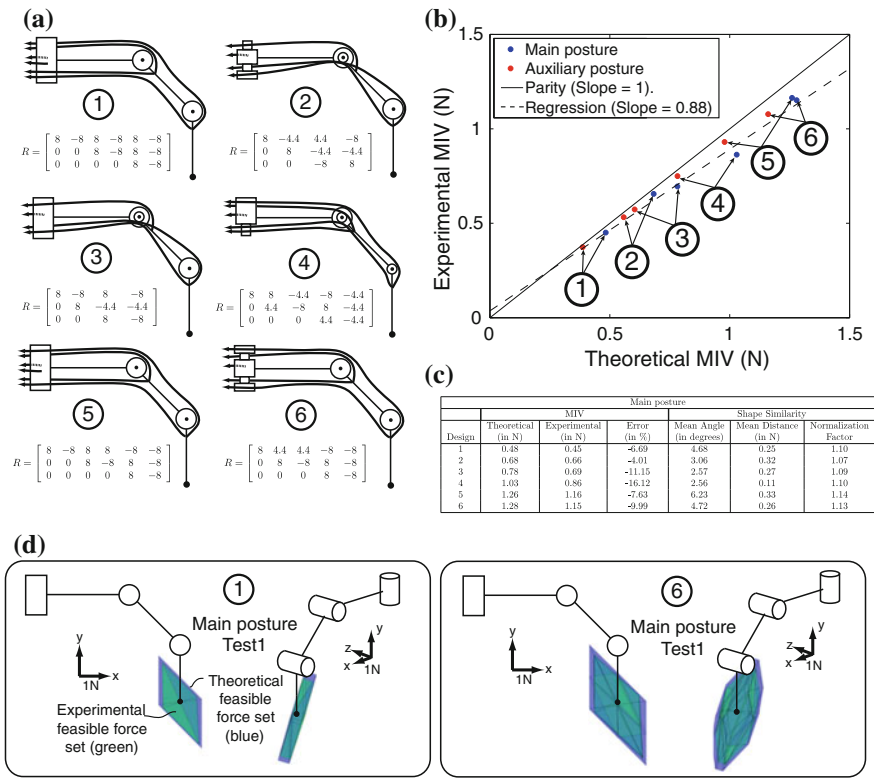


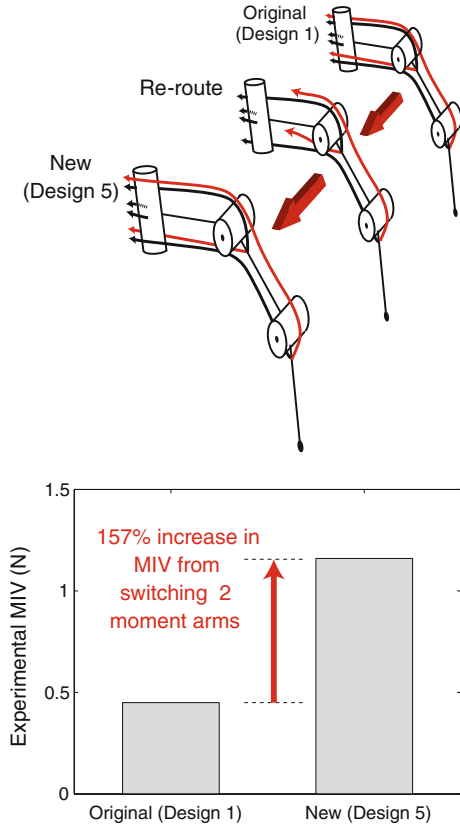
Fig. 8 Results from experimental testing of various routings. **a** The 6 different routings tested. Shown to scale. R matrix values are in mm. **b** Experimental versus theoretical MIV. Parity line is where experimental MIV would be exactly equal to theoretical MIV (intercept of 0, slope of 1). Regression has an R^2 value of 0.987. **c** Table of averages from 3 tests for each design in main posture. **d** 3-D visualization of experimental and theoretical feasible force sets for designs 1 and 6

results for each design/posture combination were extremely repeatable. We see a consistent linear relationship between theoretical and experimental MIVs with an R^2 value of 0.987. This result shows that the theoretical calculations are very good at predicting actual performance. The slope of the line is 0.879, which we interpret to represent an average loss of performance of about 12 % from theoretical predictions, likely due mainly to friction in the system. We show experimental and theoretical feasible force sets for one test of designs 1 and 6 in the main posture in Fig. 8d, and we can see visually that the shape of the theoretical feasible force sets was extremely similar to those of the experimental feasible force sets, although the experimental ones were contracted to an extent.

We can see several interesting features in Fig. 8. First of all, in Fig. 8a, we see that routings 1 and 5 are identical except that 2 of the signs in the moment arm matrix are reversed (i.e., 2 of the tendons are switched from one side of the abduction joint to the other). However, we can see in Fig. 8b and the table in Fig. 8c that the MIV of routing 5 is more than twice that of routing 1 both theoretically and experimentally. Figure 9 emphasizes this large change in MIV for a small, intelligent (but perhaps counterintuitive before performing the analyses) change in tendon routing. Secondly, the MIVs of routings 5 and 6 are very similar, but routing 6 has one less tendon. Thirdly, routings 2 and 3 have two fewer tendons than routing 1 but still outperform it in terms of MIV. Figure 8d demonstrates visually that the experimental feasible force sets corresponded very closely with the theoretical feasible force sets in shape, and that the size was similar but contracted by a small amount due to friction. While the side views of both of these feasible force sets look similar, the isometric views show clearly that the feasible force set of routing 1 is quite thin along one direction (which results in a low MIV) and the feasible force set of routing 6 is much more expanded in all directions (so the MIV is much higher).

In Fig. 8b, we see that the data points lie underneath but fairly close to the parity line (if the theoretical and experimental MIVs were identical, the data points would lie exactly on the parity line). As would be expected, none of them are above the parity line. In the table in Fig. 8c, we see that the error in the prediction of MIV ranged roughly between 4 % and 16 % which is the percentage MIV below the parity line where the data points are located. As far as shape goes, we see that the average difference in angles between corresponding vertices of the feasible force sets was between 2.56° and 6.5° . A small amount of angular error would be expected due to error in the positioning and alignment of the JR3 axes relative to the finger axes, so this contributes to the average difference in angles. The mean distance of corresponding vertices is less than 0.35N. The normalization factors were less than 1.15, and it is the factor by which the experimental feasible force set had to be expanded in every direction to have the same volume as the theoretical feasible force set. It roughly corresponds with the MIV error.

Fig. 9 Illustration of a simple (but intelligent) tendon re-routing that drastically increases MIV



6 Discussion

In this work, we have investigated the effect of various tendon routings on the set of feasible forces that can be exerted by a robotic finger both computationally and in a physical system. We see that routing has a very dramatic effect on the shape and size of the feasible force set. We also see that computational predictions are quite accurate and that they can be useful when making informed design decisions. Therefore the main conclusions of this study are twofold:

- (1) Different routings in robotic fingers can result in extremely different force-production capabilities.
- (2) Theoretical feasible force set analyses predict experimental force-production performance quite well and therefore they are a useful design tool.

One application of this work is to design tendon-driven fingers and manipulators for a given task that are optimized in terms of minimal size, weight, complexity, and cost. Since tendon-driven systems are linear for fixed postures, if we

double all the moment arms (or the maximal tensions of all tendons), we double the size of feasible force set in every direction. Our results showed that the MIV for routing 6 was more than 100 % greater than that of routing 1. Therefore, one could either reduce all of the maximal tendon tensions or all of the moment arms in routing 6 by 50 % and still have a greater MIV than routing 1. In a robotic hand system, if the maximal tendon tensions were cut in half (by implementing smaller motors), then the weight of the actuators could be roughly halved and cost would be reduced. This would be very desirable, in general. If tendons are driving a minimally-invasive surgical instrument, then the moment arms could be halved and therefore the diameter of the instrument would be halved (which actually would reduce the cross-sectional area by 75 %!). The instrument would then be much smaller and could be much better suited for certain surgical procedures.

We have used MIV as the fitness metric for our analyses since no prior assumption of task specification was made. We acknowledge that in general, the MIV would typically be more practically used for a tendon-driven, multi-purpose manipulator rather than a robotic finger. These analyses and optimizations that we described apply equally to tendon-driven manipulators and fingers regardless of size. Since we were only testing one finger in this paper, we decided to use the MIV. Current work has accomplished design optimization and validation for grasp quality of multiple fingers of identical design to the one in this chapter [47].

If a necessary task or set of tasks is known (e.g., to have high flexion force for strong grasps) then the analyses could assign a fitness metric to a routing based on that task specification. The optimization could then be based on that metric. For example, if it is desired to have a very strong flexion force with low extension force requirements, then linear programming can easily be used to determine the maximal force possible in the flexing direction(s) after the feasible force set has been calculated (e.g., using the generic procedure outlined in [24]). We have previously described that the feasible force sets of the human fingers are asymmetrically biased towards endpoint forces in the flexion direction than in the extension which is anatomically reasonable for grasping tasks [34, 48–50]. If strong grasp and minimal size/weight/cost is desired for a set of fingers, then analyses like those used in [51] can be used to design an optimized tendon-driven robotic hand.

We have investigated force-production capabilities in this paper, but there are many other considerations that go into the design of a robotic hand. Other significant considerations include the robustness and effectiveness of control algorithms, passive stiffness characteristics, sensitivity to friction and positioning errors, and maximal endpoint velocities. We acknowledge that force-production capabilities are only one piece of the design puzzle for optimized robotic fingers.

For reasons of practicality, we only analyzed and constructed routings where the tendons routed around every joint that they passed (i.e., that the structure matrix is pseudo-triangular, as in [22]) and where there were only two sizes of pulleys that could be chosen. Routings can, however, be designed where tendons pass through the center of joints [52], or where moment arms can have many feasible magnitudes. This opens up the design space even more, and exhaustive

searches like the ones we performed in this study may be more laborious, or even not be feasible given the exponential growth of design options. In addition, tendon-driven fingers or manipulators with more than 3 degrees of freedom will tend to suffer from the curse of dimensionality in the design space, and a designer may have to use various optimization algorithms [1] in a search for a “good enough” design which could then be selected for physical construction. Alternatively, a designer could come up with a handful of feasible, physically-realizable routings and then search in the vicinity of that region of the parameter space to determine feasible improvements with affordable computational cost [53].

The optimization process we used in this study only addressed this realization of a robotic finger. If a general robotic finger or manipulator has more joints or tendons, the dimensionality of the design space increases dramatically and finding a globally optimum solution for a specific fitness metric (of which any task-specific metric may be used, not only the general MIV metric) may be computationally infeasible due to the curse of dimensionality. Other custom or typical optimization algorithms could be used to find solutions with a high fitness. Furthermore, in the case when the optimization may involve link lengths and D-H parameters in addition to tendon routing, number of tendons, and pulley sizes, then finding a locally optimal solution or just a good-enough solution could still be very useful. The main purpose of this study was to investigate the correlation of predictions with experiments, as opposed to identifying a general optimization method for tendon-driven robotic fingers and manipulators.

Tendon friction was a significant factor in our experiment, (as it is for any tendon driven system), especially for the tendons at the last joint that had to wrap around as many as 12 pulleys. The main source of friction seemed to be the pulleys, as general observation of the data indicated that tendons attached to the ad-abduction joint (which wrapped around 4 pulleys) suffered from very little friction loss (less than a few %) while the tendons that attached to the last joint (which wrapped around 12 pulleys and routed through the fairly complicated tendon redirection between the first and second joints) suffered from as much as 20 % friction loss.

Future work will extend this experimental validation approach to routings of multiple fingers for optimized grasp quality. In addition, this work is easily applicable to refine the design of generic tendon-driven manipulators. Furthermore, investigation of the control and structure of biological tendon-driven systems is now made possible using a similar framework.

7 Conclusions

We conclude from this validation that these computational methods are effective at predicting the performance of drastically different tendon-driven robotic finger (or manipulator) designs, and are therefore a useful design tool. Various benefits of fully utilizing this design tool include:

- (1) *Minimization of weight*: if a superior design has a force-production performance twice that of an inferior design, the superior design's actuators only need to be half the strength of the inferior design's to match the inferior design's performance, which in general corresponds to a large reduction in weight of the actuators.
- (2) *Minimization of size*: if a superior design has a force-production performance twice that of an inferior design, the superior design's moment arms only need to be half the size of the inferior design's to match the inferior design's performance, which could be used to half the overall thickness of the finger (or manipulator, or minimally-invasive surgical device).
- (3) *Minimization of number of tendons (and therefore actuators)*: If a design with less tendons (such as an $N + 1$ design) can be synthesized with the same force-production performance as that of one with more tendons (such as a $2N$ design), then the actuator system can be simplified and less space to route the tendons inside the finger (or manipulator, or minimally-invasive surgical device) is needed.

Acknowledgments The authors gratefully acknowledge the help of Dr. Manish Kurse in providing the data acquisition routine for the experimental procedure, and Dr. Veronica Santos for construction of the gimbal used in the experiments.

References

1. J.M. Inouye, J.J. Kutch, F.J. Valero-Cuevas, A novel synthesis of computational approaches enables optimization of grasp quality of tendon-driven hands. *IEEE Trans. Rob.* 1–9 (2012)
2. S. Jacobsen, E. Iversen, D. Knutti, R. Johnson, K. Biggers, Design of the utah/mit dextrous hand. *IEEE Int. Conf. Rob. Autom.* **3**, 1520–1532 (1986)
3. J.K. Salisbury, J.J. Craig, Articulated hands: Force control and kinematic issues. *Int. J. Robot. Res.* **1**(1), 4 (1982)
4. Shadow Dexterous Hand, Shadow Robot Company
5. M. Grebenstein, A. Albu-Schffer, T. Bahls, M. Chalon, O. Eiberger, W. Friedl, R. Gruber, U. Hagn, R. Haslinger, H. Hppner, The dlr hand arm system, Submitted to ICRA, vol. 11
6. R.O. Ambrose, H. Aldridge, R.S. Askew, R.R. Burrige, W. Bluethmann, M. Diftler, C. Lovchik, D. Magruder, F. Rehnmark, Robonaut: Nasa's space humanoid. *IEEE Intell. Syst. Appl.* **15**(4), 57–63 (2000)
7. B.M. Jau, Dexterous telemanipulation with four fingered hand system, in *Proceedings of IEEE International Conference on Robotics and Automation*, vol. 1, pp. 338–343, 1995
8. B. Massa, S. Roccella, M.C. Carrozza, P. Dario, Design and development of an underactuated prosthetic hand, in *Proceedings of IEEE International Conference on Robotics and Automation (ICRA '02)*, vol. 4, pp. 3374–3379, 2002
9. L.R. Lin, H.P. Huang, Mechanism design of a new multifingered robot hand, in *Proceedings of 1996 IEEE International Conference on Robotics and Automation*, vol. 2, pp. 1471–1476, 1996
10. H. Kawasaki, T. Komatsu, K. Uchiyama, Dexterous anthropomorphic robot hand with distributed tactile sensor: Gifu hand II. *IEEE/ASME Trans. Mechatronics* **7**(3), 296–303 (2002)

11. A. Namiki, Y. Imai, M. Ishikawa, M. Kaneko, Development of a high-speed multifingered hand system and its application to catching, in *Proceedings of 2003 IEEE/RSJ International Conference on Intelligent Robots and Systems (IROS 2003)*, vol. 3, pp. 2666–2671, 2003
12. I. Yamano, T. Maeno, Five-fingered robot hand using ultrasonic motors and elastic elements, in *Proceedings of the 2005 IEEE International Conference on Robotics and Automation (ICRA 2005)*, pp. 2673–2678, 2005
13. I. Gaiser, S. Schulz, A. Kargov, H. Klosek, A. Bierbaum, C. Pylatiuk, R. Oberle, T. Werner, T. Asfour, G. Bretthauer, A new anthropomorphic robotic hand, in *Proceedings of 8th IEEE-RAS International Conference on Humanoid Robots*, pp. 418–422, 2008
14. J.L. Pons, R. Ceres, F. Pfeiffer, Multifingered dextrous robotics hand design and control: a review. *Robotica* **17**(6), 674 (1999)
15. F. Firmani, A. Zibil, S.B. Nokleby, R.P. Podhorodeski, Wrench capabilities of planar parallel manipulators. part I: wrench polytopes and performance indices. *Robotica* **26**(06), 791–802 (2008)
16. S. Bouchard, C.M. Gosselin, B. Moore, On the ability of a cable-driven robot to generate a prescribed set of wrenches, in *Proceedings of the ASME International Design Engineering Technical Conferences, Mechanics and Robotics Conference, Citeseer*, 2008
17. P. Chiacchio, Y. Bouffard-Vercelli, F. Pierrot, Force polytope and force ellipsoid for redundant manipulators. *J. Robot. Syst.* **14**(8), 613–620 (1997)
18. R. Finotello, T. Grasso, G. Rossi, A. Terribile, Computation of kinetostatic performances of robot manipulators with polytopes, in *Proceedings 1998 IEEE International Conference on Robotics and Automation*, vol. 4, pp. 3241–3246, 1998
19. M. Gouttefarde, S. Krut, Characterization of parallel manipulator available wrench set facets. *Adv. Robot Kinematics Motion Man Mach.* 475–482 (2010)
20. A. Zibil, F. Firmani, S.B. Nokleby, R.P. Podhorodeski, An explicit method for determining the force-moment capabilities of redundantly actuated planar parallel manipulators. *J. Mech. Des.* **129**, 1046 (2007)
21. L.W. Tsai, Design of tendon-driven manipulators. *J. Mech. Des.* **117**, 80 (1995)
22. J.J. Lee, L.W. Tsai, The structural synthesis of tendon-driven manipulators having a pseudotriangular structure matrix. *Int. J. Robot. Res.* **10**(3), 255 (1991)
23. J.J. Lee, Tendon-driven manipulators: analysis, synthesis, and control. Ph.D Dissertation, University of Maryland, 1991
24. J.L. Fu, N.S. Pollard, On the importance of asymmetries in grasp quality metrics for tendon driven hands, in *Proceedings of 2006 IEEE/RSJ International Conference on Intelligent Robots and Systems*, pp. 1068–1075, 2006
25. D.Z. Chen, J.C. Su, K.L. Yao, A decomposition approach for the kinematic synthesis of tendon-driven manipulators. *J. Robot. Syst.* **16**(8), 433–443 (1999)
26. Y.J. Ou, L.W. Tsai, Kinematic synthesis of tendon-driven manipulators with isotropic transmission characteristics. *J. Mech. Des.* **115**, 884 (1993)
27. Y.J. Ou, L.W. Tsai, Isotropic design of tendon-driven manipulators. *J. Mech. Des.* **118**(3), pp. 360–366 (1996)
28. J.B. Sheu, J.J. Huang, J.J. Lee, Kinematic synthesis of tendon-driven robotic manipulators using singular value decomposition. *Robotica* **28**(01), 1–10 (2009)
29. J. Angeles, *On the Optimum Dimensioning of Robotic Manipulators* (McGill University, Montreal, 2004)
30. M.M. Aref, H.D. Taghirad, S. Barissi, Optimal design of dexterous cable driven parallel manipulators. *Int. J. Robot. Theory Appl.* **2**(4), 43–51 (2009)
31. D. Chablat, J. Angeles, On the kinetostatic optimization of revolute-coupled planar manipulators. *Mech. Mach. Theory* **37**(4), 351–374 (2002)
32. W.A. Khan, J. Angeles, The kinetostatic optimization of robotic manipulators: the inverse and the direct problems. *J. Mech. Des.* **128**, 168 (2006)
33. L. Kuxhaus, S.S. Roach, F.J. Valero-Cuevas, Quantifying deficits in the 3d force capabilities of a digit caused by selective paralysis: application to the thumb with simulated low ulnar nerve palsy. *J. Biomech.* **38**(4), 725–736 (2005)

34. F.J. Valero-Cuevas, F.E. Zajac, C.G. Burgar, Large index-fingertip forces are produced by subject-independent patterns of muscle excitation. *J. Biomech.* **31**(8), 693–704 (1998)
35. F.J. Valero-Cuevas, A mathematical approach to the mechanical capabilities of limbs and fingers. *Prog. Mot. Control* 619–633 (2005)
36. F.J. Valero-Cuevas, V.V. Anand, A. Saxena, H. Lipson, Beyond parameter estimation: extending biomechanical modeling by the explicit exploration of model topology. *IEEE Trans. Biomed. Eng.* **54**, 1951–1964 (2007)
37. J.M. Inouye F.J. Valero-Cuevas, Asymmetric routings with fewer tendons can offer both flexible endpoint stiffness control and high force-production capabilities in robotic fingers, in *Proceedings of the Fourth IEEE RAS/EMBS International Conference on Biomedical Robotics and Biomechanics (BioRob)*, Rome, 2012
38. F.J. Valero-Cuevas, An integrative approach to the biomechanical function and neuromuscular control of the fingers. *J. Biomech.* **38**, 673–684 (2005)
39. J.J. Kutch, F.J. Valero-Cuevas, Muscle redundancy does not imply robustness to muscle dysfunction. *J. Biomech.* **44**(7), 1264–1270 (2011)
40. J.J. Kutch, F.J. Valero-Cuevas, Challenges and new approaches to proving the existence of muscle synergies of neural origin. *PLoS Comput. Biol.* **8**(5), <http://www.ncbi.nlm.nih.gov/pmc/articles/PMC2257060/>. Accessed May 2012
41. C.B. Barber, D.P. Dobkin, H. Huhdanpaa, The quickhull algorithm for convex hulls. *ACM Trans. Math. Softw.* **22**(4), 469–483 (1996)
42. K. Fukuda, A. Prodon, Double description method revisited. *Comb. Comput. Sci.* **1120**, 91–111 (1996)
43. D. Avis, in *Polytopes—combinatorics and computation* ed. by G. Kalai, G. Ziegler. A Revised Implementation of the Reverse Search Vertex Enumeration Algorithm, vol. 29 (Birkhauser-Verlag, DMV Seminar Band 29, 2000), pp. 177–198
44. J. Butterfahl, M. Grebenstein, H. Liu, G. Hirzinger, Dlr-hand II: next generation of a dextrous robot hand, in *Proceedings 2001 ICRA IEEE International Conference on Robotics and Automation*, vol. 1 (IEEE, 2001), pp. 109–114
45. N.S. Pollard, R.C. Gilbert, Tendon arrangement and muscle force requirements for humanlike force capabilities in a robotic finger. *Environment* **17**, 14 (2002)
46. G. Taguchi, S. Konishi, *Orthogonal Arrays and Linear Graphs: Tools for Quality Engineering* (American Supplier Institute, Allen Park, 1987)
47. J.M. Inouye, Bio-inspired tendon-driven systems: computational analysis, optimization, and hardware implementation. Ph.D. Dissertation, University of Southern California, 2012
48. J.M. Inouye, J.J. Kutch, F. Valero-Cuevas, Quantitative prediction of grasp impairment following peripheral neuropathies of the hand, in *Proceedings of the 35th Annual Meeting of the American Society of Biomechanics*, Long Beach, CA, 2011
49. F.J. Valero-Cuevas, J.D. Towles, V.R. Hentz, Quantification of fingertip force reduction in the forefinger following simulated paralysis of extensor and intrinsic muscles. *J. Biomech.* **33**(12), 1601–1609 (2000)
50. F.J. Valero-Cuevas, V.R. Hentz, Releasing the A3 pulley and leaving flexor superficialis intact increases pinch force following the zancolli lasso procedures to prevent claw deformity in the intrinsic palsied finger. *J. Orthop. Res.* **20**(5), 902–909 (2002)
51. J.M. Inouye, J.J. Kutch, F. Valero-Cuevas, A novel methodology to compare grasp quality: application to two dominant tendon-driven designs, in *Proceedings of the 35th Annual Meeting of the American Society of Biomechanics*, Long Beach, CA, 2011
52. M. Grebenstein, M. Chalou, G. Hirzinger, R. Siegart, Antagonistically driven finger design for the anthropomorphic dlr hand arm system, in *Proceedings of IEEE-RAS International Conference on Humanoid Robots (HUMANOIDS)*, 2010
53. F.J. Valero-Cuevas, H. Hoffmann, M.U. Kurse, J.J. Kutch, E.A. Theodorou, Computational models for neuromuscular function. *IEEE Rev. Biomed. Eng.* **2**, 110–135 (2009)